# Intrinsically Switchable GHz Ferroelectric ScAlN SAW Resonators

Ved Gund<sup>1</sup>, Kazuki Nomoto<sup>1</sup>, Huili Grace Xing<sup>1,2,3</sup>, Debdeep Jena<sup>1,2,3</sup>, and Amit Lal<sup>1</sup>

<sup>1</sup>Electrical and Computer Engineering Cornell University Ithaca, NY, USA <sup>2</sup>Materials Science and Engineering Cornell University Ithaca, NY, USA <sup>3</sup>Kavli Institute at Cornell Cornell University Ithaca, NY, USA

Abstract — This paper reports on the intrinsic switching of GHz ferroelectric scandium aluminum nitride (ScAlN) surface acoustic wave (SAW) resonators. The reversible switching was demonstrated on 22% and 30% ScAIN for frequencies in the 1-3 GHz range, with metal interdigitated transducers (IDTs) of widths 1 µm-400 nm patterned with electron-beam lithography. COMSOL simulations were used to model resonator programming, with ScAlN switching under the IDTs. The devices show strong resonances with a quality factor of 915 and a coupling coefficient of 0.98% at 1.35 GHz. Two-state switching of the resonator is demonstrated with single-sided pulses of  $\pm$  6 MV/cm, which demonstrates reversible on and off switching of piezoelectricity in ScAlN. Progressively larger switching pulses in the  $\pm$  (2-5) MV/cm range demonstrate multi-state switching of the SAW device by tracking the S-parameters and quality factor. The results presented in this paper open up pathways towards programmable signal processing and sensing using ferroelectric ScAIN.

Keywords – Intrinsic Switching, Aluminum Scandium Nitride, ScAlN, SAW resonator, Ferroelectric, CMOS-compatible

# I. INTRODUCTION

Radio frequency frontend modules (RF-FEMs) for wireless communications have been significantly enabled by key technological progress in III-V nitride-based materials such as gallium nitride (GaN) for power electronics and switches, and aluminum nitride (AlN) for signal processing and filtering with the film bulk acoustic resonator (FBAR) [1]–[3]. Lithium niobate (LiNbO<sub>3</sub>) and lithium tantalate (LiTaO<sub>3</sub>) have been used to achieve high performance RF filters with surface acoustic wave (SAW) resonators, which enable lithographic control of the filter frequency [4], [5]. Today, the definition of modern 5G and 6G communication standards has resulted in a crowded frequency spectrum, which necessitates both high performance operation, and reconfigurable and adaptive RF-FEMs with tunable filters and controllable signal jamming and transmission [6].

Improved filter performance can be achieved with scandium-doped AlN (ScAlN) filters, which can improve the piezoelectric coupling coefficients of AlN by up to 4 times [7]. As a result, high performance bulk and SAW resonators have been demonstrated using ScAlN [8]–[10]. To demonstrate reconfigurable and adaptive filtering, it is highly desirable to achieve programmable piezoelectric coupling in ScAlN, which can then be used to tune the frequency and transmission level of the filter. Fichtner et al. have shown that high scandium fraction incorporation in ScAlN (20-40%) makes it ferroelectric by reducing the coercive field ( $E_C$ ) needed for polarization switching, below the breakdown field ( $E_{BD}$ ) [11]. Ferroelectric ScAlN has a box-like polarization vs E-field (PE) loop, which is attractive for applications in programmable memory and signal processing for tunable

filters. One of the challenges with device-level utilization of ferroelectricity in ScAlN is the high  $E_{\rm C}\sim 4\text{--}5~\text{MV/cm}$  which necessitates large voltages for polarization switching, even in 200-300 nm films. We have previously reported on the ferroelectric properties of various ScAlN compositions across a range of device sizes, templating electrodes, film stress, and frequency of switching with a goal of identifying reduced switching voltages, including a reduction in the coercive field by 37% with heating up to 193  $^{0}\text{C}$  [12], [13]. Polarization switching in bulk and laminate film ScAlN acoustic wave devices has been previously reported [10], [14], [15]. However, to our knowledge, there are no published reports on intrinsic polarization switching in ScAlN SAW resonators.

# II. DEVICE DESIGN

# A. Ferroelectric SAW Resonator

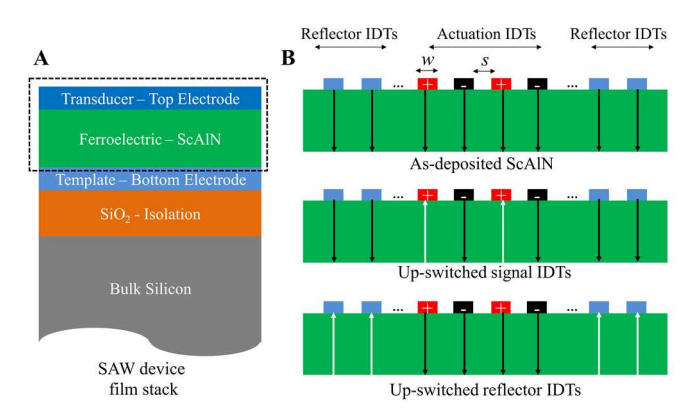


Figure 1: A). Thin-film stack used for the SAW device consisting of an SiO<sub>2</sub> isolation layer, template bottom electrode, wurtzite c-axis ferroelectric ScAlN, and top electrodes for SAW actuation. B). Schematic cross-section of the transducer IDTs and ferroelectric ScAlN showing three distinct configurations of ScAlN polarization: as-deposited N-polar ScAlN with uniform polarization pointing downward, up-switched ScAlN under signal IDTs to program piezoelectric coupling in the active region, up-switched ScAlN under reflector IDTs to program acoustic wave boundary conditions.

Figure 1A shows the cross-section of the film stack used to make the resonator comprising: a continuous bottom electrode which serves as the template, c-axis wurtzite ScAlN of thickness  $t_{ScAlN}$ , and the top electrode for patterning the SAW IDTs. The IDTs with width w and spacing s enable lithographic definition of the resonance wavelength:

$$\lambda = 2(w + s)$$

The passive reflector electrodes enable effective energy confinement in the acoustic cavity defined by the IDTs. For as-deposited N-polar ScAlN, the polarization points downwards. As such, it is possible to switch the polarization of ScAlN under signal electrode IDTs, ground electrode IDTs,

reflectors, or a combination of these for local tuning of the piezoelectric coupling, to program the resonator frequency and  $S_{11}$  reflection coefficient as shown in Figure 1B.

# B. Analytical Modeling and COMSOL Simulations

The key design considerations for a ferroelectric SAW resonator are the switching voltage  $V_C$  and the electromechanical coupling coefficient  $k_t^2$  (Figure 2).  $V_C$ scales linearly with  $t_{ScAIN}$ . As such, thinner ScAIN enables lower switching voltages:

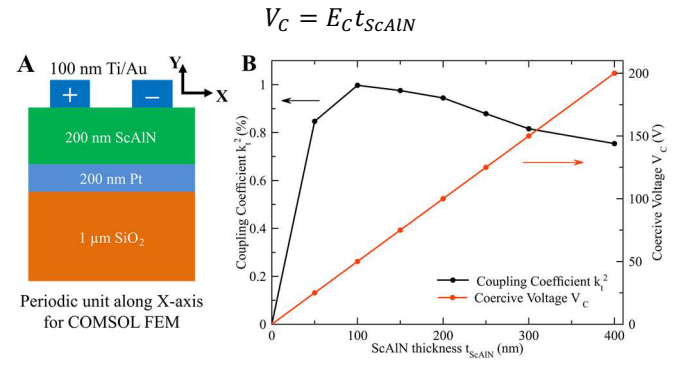


Figure 2: A). Periodically repeating unit cell along the X-axis for COMSOL modeling to simulate  $k_t^2$  and ferroelectric switching. B). ScAlN thickness-dependence of the coercive voltage  $V_C$  (for  $E_C = 5$ MV/cm) and simulated coupling coefficient  $k_t^2$  for the film-stack.

COMSOL finite element modeling (FEM) was performed to determine the non-linear dependence of  $k_t^2$  on  $t_{ScAlN}$  using a unit cell of the SAW device with periodic boundary conditions. For a SAW device with  $\lambda = 1.6 \,\mu m$ , the maximum simulated value of  $k_t^2 = 0.99\%$  was achieved for  $t_{ScAlN} = 100 \, nm$ . Unlike conventional SAW devices which are made on thick substrates  $\gg$   $\lambda$  and without a bottom electrode, the need to: 1). reduce  $V_C$  and 2). template c-axis ScAlN necessitate the chosen thin-film stack. To template high crystal quality ScAlN while maintaining a sufficiently large  $k_t^2$  and to avoid using extremely large voltages,  $t_{SCALN} =$ 200 nm was used for devices in this paper.

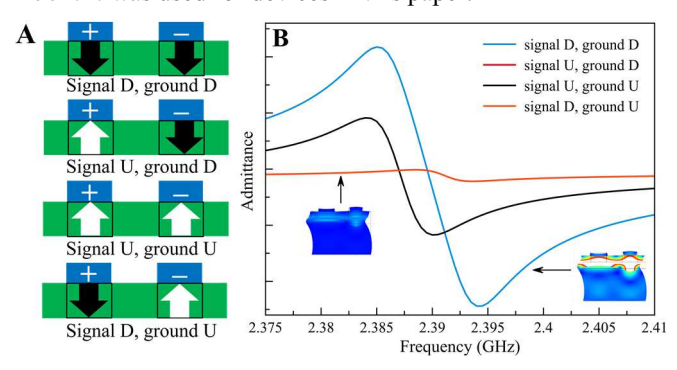


Figure 3: A). SAW resonator polarization configurations with ScAlN under the signal and ground IDTs switched up or down, denoted by U and D, and shown with black and white arrows respectively. B). Simulated admittance of each configuration showing a resonant response for as-fabricated SAW devices and suppression of the resonance with signal or ground IDT up-switching. The inset mode shapes show relative displacement for high and low piezoelectric coupling. The ScAlN polarization in the regions without metal coverage is assumed to be down-switched in all 4 configurations.

COMSOL was also used to simulate and verify the SAW resonator programming due to polarization switching. Figure 3 shows admittances for 4 distinct polarization states. Asfabricated devices with uniform polarization pointing downwards (signal D, ground D) show a resonant admittance response. With ScAlN polarization switching under either of the signal or ground electrodes (signal U, ground D or signal D, ground U), the resonance is almost completely suppressed, resulting in a capacitive response. This result can be explained as an averaging effect of the alternating opposingly poled ScAlN under the signal and ground electrodes that leads to an average near-zero piezoelectric coupling in the SAW resonator cavity. For up-switched ScAlN under both sets of IDTs (signal U, ground U), both, a frequency shift and resonance amplitude change are observed.

# III. EXPERIMENTAL RESULTS

# A. SAW Resonator Fabrication

200 nm ScAlN films with 22% and 30% doping were deposited on continuous Pt and Mo bottom electrodes respectively by reactive co-sputtering (Sc) of scandium and aluminum (Al) in nitrogen. A double-layer lift-off process was to evaporate 10 nm/100 nm Ti/Au metal electrodes with contact pads, routing lines, and test capacitors patterned using contact photolithography (smallest features =  $3 \mu m$ ), and the metal IDTs patterned using electron-beam lithography. The IDT width w were designed to be from 1 μm down to 400 nm, corresponding to target SAW frequencies in the 1-3 GHz range for the two ScAlN compositions. Figure 4 shows a scanning electron microscope (SEM) image and zoom-in of a ScAlN SAW device with 400 nm IDTs including a process simulation with MEMSPro to verify high-fidelity contact with the 2-layer evaporation.

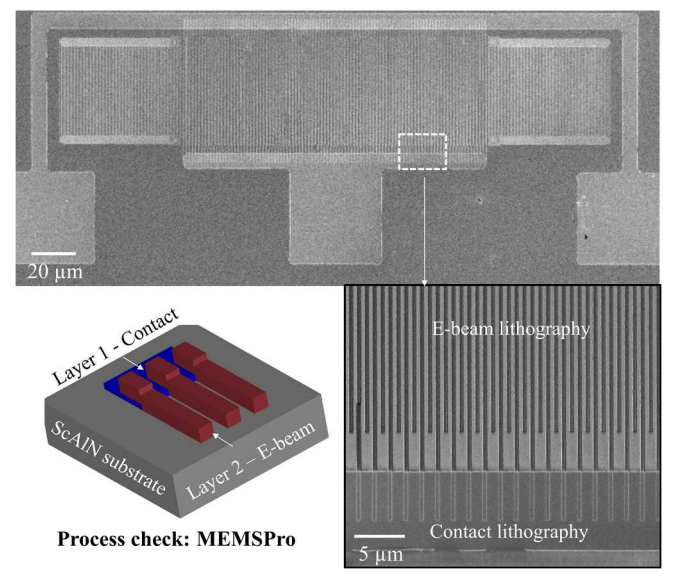


Figure 4: SEM image of a SAW device with 400 nm IDTs, including a zoom-in view of the overlapping metal layers patterned with ebeam and contact lithography. A 3D isometric view serves as a process check to confirm high-fidelity contact between the two layers.

# B. SAW Resonator Characterization

A network analyzer (Keysight E5061B) was used to measure  $S_{11}$  amplitude and phase of SAW devices on 30% ScAlN with Mo bottom electrode. Figure 5 shows data for 1  $\mu$ m and 400 nm SAW IDTs with resonances at 1.35 and 2.75 GHz respectively. The 1.35 GHz resonator has a high Q-factor (Q = 915) as determined from the expression below [16]:  $Q = \omega \left(\frac{d\phi}{d\omega}\right) \left(\frac{|S_{11}|}{1 - |S_{11}|^2}\right)$ 

$$Q = \omega \left(\frac{d\phi}{d\omega}\right) \left(\frac{|S_{11}|}{1 - |S_{11}|^2}\right)$$

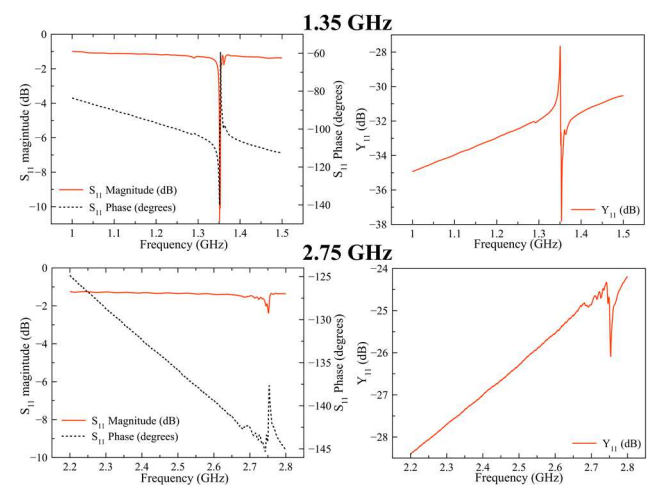


Figure 5:  $S_{11}$  amplitude and phase, and  $Y_{11}$  admittance plots for 30% ScAlN SAW devices with 1  $\mu$ m (top) & 400 nm (bottom) IDTs.

Here,  $\omega$  and  $\frac{d\phi}{d\omega}$  are the angular frequency and group delay. The measured values of  $k_t^2$  at 1.35 and 2.75 GHz are 0.54% and 0.98% respectively, in close agreement with simulated values. Table 1 summarizes the performance of the devices.

Table 1: Frequency, coupling coefficient, and quality factor for 1 µm and 400 nm IDT devices on 200 nm 22% ScAlN

IDT width	Frequency	Coupling	Quality
w (µm)	(GHz)	coefficient $k_t^2$ (%)	Factor Q
1	1.35	0.54	915
0.4	2.75	0.98	226

# C. ScAlN Ferroelectric Characterization

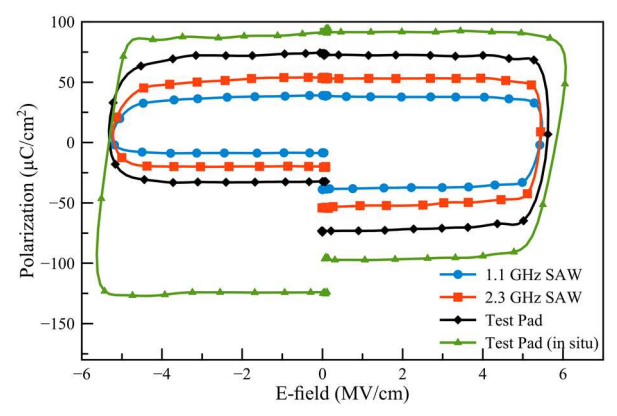


Figure 6: Polarization vs. E-field (PE) loops for 1.1 and 2.3 GHz SAW devices and a test pad on 22% ScAlN. The devices in this paper show lower remnant polarization in comparison with an in situ deposited metal pad (outer green loop), potentially due to surface oxidation as a result of exposure to ambient oxygen.

Ferroelectric characterization of 22 % ScAlN was done for 1.1 and 2.3 GHz SAW devices, and a 40  $\mu$ m diameter test pad. A Sawyer-Tower circuit with a continuous wave (CW) 1 kHz positive-up-negative-down (PUND) input was used for ferroelectric wake-up of the tested devices, using a 11.8 k $\Omega$  series resistor to measure switching and leakage currents. The coercive field and remnant polarization pairs ( $E_C$ ,  $P_r$ ) for the 1.1 and 2.3 GHz SAW devices were (5.4 MV/cm, 38.9  $\mu$ C/cm<sup>2</sup>) and (5.4 MV/cm, 53.6  $\mu$ C/cm<sup>2</sup>) respectively, lower than that of a 50  $\mu$ m x 50  $\mu$ m test capacitor (5.6 MV/cm, 72.5  $\mu$ C/cm<sup>2</sup>). This indicates incomplete saturation, likely due to

the 2-3x larger area of the SAW devices and large access resistance of the IDTs. For reference, an in situ deposited metal pad on ScAlN has a larger remnant polarization than the SAW devices, a likely consequence of ScAlN surface oxidation because of exposure to the ambient.

# D. SAW Intrinsic Ferroelectric Switching

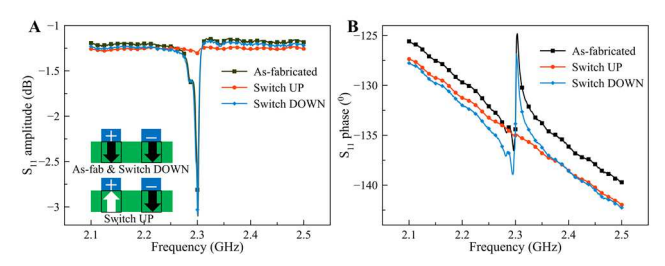


Figure 7: A).  $S_{11}$  amplitude (in dB) and B). phase (in  $^{0}$ ) for a 2.3 GH 22% ScAlN SAW resonator showing two-state ScAlN programming. The as-fabricated, up-switched, and down-switched responses demonstrate reversible polarization switching, which enables turning off of the piezoelectric coupling and its full recovery to demonstrate a programmable resonator.

Two-state ScAlN programming (hard-switching): Single-sided triangular pulses of  $\pm\,6$  MV/cm (larger than the coercive field), were applied to the SAW signal IDTs to sequentially up-switch and down-switch the ScAlN underneath them, followed by  $S_{11}$  measurements after each switching cycle. Figure 7 shows  $S_{11}$  amplitude and phase responses of a 2.3 GHz 22% ScAlN SAW device for as-fabricated, up-switched (–6 MV/cm pulses), and down-switched (+6 MV/cm pulses) cases. Consistent with COMSOL modeling, the resonance vanishes with up-switching of ScAlN due to an average turning off of piezoelectricity in the device but is fully recovered with down-switching. This process is repeatable over multiple cycles, demonstrating reversible intrinsic switching of the resonator with minimal degradation.

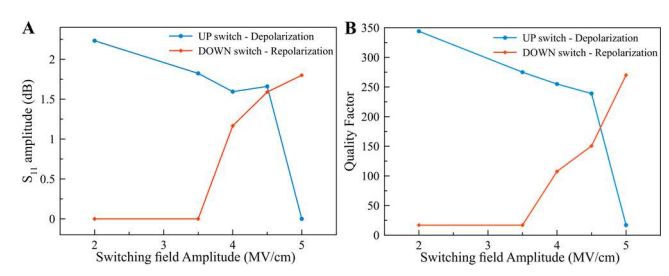


Figure 8: A).  $S_{11}$  amplitude (in dB) and B). Q-factor as a function of increasing up and down switching fields between 2-5 MV/cm on ScAlN.  $S_{11}$  and Q, both decrease with up-switching due depolarization with a dramatic decrease at 5 MV/cm, followed by a nearly complete recovery with repolarization via down-switching.

Multi-state programming (partial-switching): Progressively larger negative pulses from –2 to –5 MV/cm were applied to the signal IDTs to partially up-switch 22% ScAlN. This was followed by down-switching with increasing positive pulses from 2 to 5 MV/cm. The RF response of the SAW device was measured after each switching input (Figure 8). The amplitude of the S<sub>11</sub> reflection is observed to progressively decrease with large negative amplitudes, with a sharp drop at –5 MV/cm which indicates depolarization of the SAW device (Figure 8A). By applying increasing positive pulses, the ScAlN is progressively down-switched which repolarizes the device and recovers the resonant response of the SAW. The depolarization and repolarization are also reflected in the Q-factor of the SAW, which decreases with up-switching (from

344 to 17) and increases with down-switching (from 17 to 270). The incomplete recovery of  $S_{11}$  and the Q-factor can be attributed to partial degradation of the ScAlN during the > 10,000 switching pulses applied with the CW switching setup.

# IV. CONCLUSIONS

Intrinsic ferroelectric switching of 1-3 GHz ScAlN SAW resonators has been demonstrated for 22% and 30% ScAlN. The polarization switching is able to completely turn off as well as fully recover the piezoelectricity in the SAW device. Hence, the paper demonstrates a programmable resonator towards reconfigurable and adaptive filters. Two-state and multi-state switching of the ScAlN present a viable pathway towards a CMOS-compatible programmable filter with frequency and amplitude control. The ability to track S<sub>11</sub> and Q-factor as a function of progressively larger switching fields also opens up opportunities for using highly-doped ScAlN for programmable signal processing and sensing applications.

# V. ACKNOWLEDGMENTS

This work was performed in part at the Cornell NanoScale Facility (CNF), an NNCI member supported by NSF Grant NNCI-2025233 and made use of the Cornell Center for Materials Research (CCMR) Shared Facilities which are supported through the NSF MRSEC program (DMR-1719875). The authors thank Dr. Joe Casamento, Shubham Jadhav, and Dr. Ben Davaji for useful discussions. Funding was provided by the DARPA TUFEN program, monitored by Dr. Ron Polcawich and Dr. Ali Keshavarzi.

### REFERENCES

- [1] R. C. Ruby, P. Bradley, Y. Oshmyansky, A. Chien, and J. D. Larson, "Thin film bulk wave acoustic resonators (FBAR) for wireless applications," in *Proceedings of the IEEE Ultrasonics Symposium*, 2001, vol. 1, pp. 813–821, doi: 10.1109/ultsym.2001.991846.
- [2] S. N. Mohammad, A. A. Salvador, and H. Morkoç, "Emerging Gallium Nitride Based Devices," *Proc. IEEE*, vol. 83, no. 10, pp. 1306–1355, 1995, doi: 10.1109/5.469300.
- [3] R. J. Kaplar et al., "Review—Ultra-Wide-Bandgap AlGaN Power Electronic Devices," ECS J. Solid State Sci. Technol., vol. 6, no. 2, pp. Q3061–Q3066, 2016, doi: 10.1149/2.0111702jss.
- [4] M. Kadota et al., "Surface Acoustic Wave Duplexer for US Personal Communication Services with Good Temperature Characteristics," Jpn. J. Appl. Phys., vol. 44, no. 6B, pp. 4527–4531, Jun. 2005, doi: 10.1143/JJAP.44.4527/META.
- [5] M. Kadota, Y. Ishii, and S. Tanaka, "A spurious-free, steep band

- rejection filter using a LiTaO3/quartz heteroacoustic layer surface acoustic wave resonator," *Jpn. J. Appl. Phys.*, vol. 59, no. SK, p. SKKC11, May 2020, doi: 10.35848/1347-4065/AB8BC1.
- [6] K. Y. Hashimoto, S. Tanaka, and M. Esashi, "Tunable RF SAW/BAW filters: Dream or reality?," *Proc. IEEE Int. Freq. Control Symp. Expo.*, 2011, doi: 10.1109/FCS.2011.5977297.
- [7] M. Akiyama, T. Kamohara, K. Kano, A. Teshigahara, Y. Takeuchi, and N. Kawahara, "Enhancement of piezoelectric response in scandium aluminum nitride alloy thin films prepared by dual reactive cosputtering," *Adv. Mater.*, vol. 21, no. 5, pp. 593–596, Feb. 2009, doi: 10.1002/adma.200802611.
- [8] Z. Tang, M. D'Agati, and R. H. Olsson, "High Coupling Coefficient Resonance Mode in Al0.68Sc0.32N Surface Acoustic Wave Resonator with AlN Buffer Layer on a Silicon Substrate," IFCS-ISAF 2020 - Jt. Conf. IEEE Int. Freq. Control Symp. IEEE Int. Symp. Appl. Ferroelectr. Proc., Jul. 2020, doi: 10.1109/IFCS-ISAF41089.2020.9234828.
- [9] Z. Hao et al., "Single Crystalline ScAlN Surface Acoustic Wave Resonators with Large Figure of Merit (Q × k)," IEEE MTT-S Int. Microw. Symp. Dig., vol. 2019-June, pp. 786–789, Jun. 2019, doi: 10.1109/MWSYM.2019.8700824.
- [10] J. Wang, M. Park, S. Mertin, T. Pensala, F. Ayazi, and A. Ansari, "A Film Bulk Acoustic Resonator Based on Ferroelectric Aluminum Scandium Nitride Films," *J. Microelectromechanical Syst.*, vol. 29, no. 5, pp. 741–747, Oct. 2020, doi: 10.1109/JMEMS.2020.3014584.
- [11] S. Fichtner, N. Wolff, F. Lofink, L. Kienle, and B. Wagner, "AlScN: A III-V semiconductor based ferroelectric," J. Appl. Phys., vol. 125, no. 11, p. 114103, Mar. 2019, doi: 10.1063/1.5084945.
- [12] V. Gund et al., "Temperature-dependent Lowering of Coercive Field in 300 nm Sputtered Ferroelectric Al0.70Sc0.30N," IEEE Int. Symp. Appl. Feeroelectric, ISAF 2021, Int. Symp. Integr. Funct. ISIF 2021 Piezoresponse Force Microsc. Work. PFM 2021 - Proc., May 2021, doi: 10.1109/ISAF51943.2021.9477328.
- [13] V. Gund et al., "Towards Realizing the Low-Coercive Field Operation of Sputtered Ferroelectric ScxAl1-xN," 21st Int. Conf. Solid-State Sensors, Actuators Microsystems, TRANSDUCERS 2021, pp. 1064– 1067, Jun. 2021, doi: 10.1109/TRANSDUCERS50396.2021.9495515.
- [14] B. Herrera, M. Pirro, G. Giribaldi, L. Colombo, and M. Rinaldi, "AlScN Programmable Ferroelectric Micromachined Ultrasonic Transducer (FMUT)," 21st Int. Conf. Solid-State Sensors, Actuators Microsystems, TRANSDUCERS 2021, pp. 38–41, Jun. 2021, doi: 10.1109/TRANSDUCERS50396.2021.9495581.
- [15] S. Dabas, D. Mo, S. Rassay, and R. Tabrizian, "Intrinsically Tunable Laminated Ferroelectric Scandium Aluminum Nitride Extensional Resonator Based on Local Polarization Switching," *IEEE Symp. Mass Storage Syst. Technol.*, vol. 2022-January, pp. 1050–1053, 2022, doi: 10.1109/MEMS51670.2022.9699790.
- [16] D. A. Feld, R. Parker, R. Ruby, P. Bradley, and S. Dong, "After 60 years: A new formula for computing quality factor is warranted," *Proc. IEEE Ultrason. Symp.*, pp. 431–436, 2008, doi: 10.1109/ULTSYM.2008.0105.